Modeling the Yule–Nielsen Effect on Color Halftones

J. S. Arney,* Tuo Wu and Christine Blehm*
Rochester Institute of Technology, Center for Imaging Science
Rochester, New York 14623-0887

Abstract

The Neugebauer approach to modeling color *cmy* halftones generally has to be modified to correct for the Yule–Nielsen light scattering effect. The most common modification involves the Yule–Nielsen *n* factor. A less common, but more fundamentally correct modification of the Neugebauer model involves a convolution of the halftone geometry with the point spread function, PSF, of the paper. The probability model described in the current report is less complex than the PSF convolution approach but is still much less empirical than the Yule–Nielsen *n* model. The probability model assumes the Neugebauer equations are correct and that the Yule–Nielsen effect manifests itself in a variation in the *XYZ* tristimulus values of the eight Neugebauer primary colors as a function of the amounts of *c*, *m*, and *y* printed. The model describes these color shifts as a function of physical parameters of the ink and paper that can be measured independently. The model is based on the assumption that scattering and absorption probabilities are independent, that the inks obey Beer–Lambert optics, and that ink dots are printed randomly with perfect hold-out. Experimentally, the model is most easily tested by measuring the shift in the color of the paper between the halftone dots, and experimental microcolorimetry is presented to verify the model.

Background

One of the conceptual advantages of halftoning is the linearity between the fractional area coverage of the ink dots, F_k, and the overall reflectance R of the image as expressed in the Murray–Davies equation, $R = F_k R_k + (1 - F_k)R_p$, where R_k and R_p are the reflectance factors of the ink and paper, respectively. In color halftoning this also means a linearity between c, m, and y dot areas and the CIE *XYZ* chromaticity coordinates of the image. However experimental measurements typically show a nonlinearity between R and F_k with R being less than predicted by the Murray–Davies equation. The nonlinearity between F_k and R is caused by two phenomena: (1) physical dot gain in which the actual dot fraction is larger than the dot fraction commanded in the printing process, and (2) the Yule–Nielsen effect in which the lateral scatter of light within the paper leads to an increase in the probability of the ink dots absorbing the light.[1] Thus, to describe tone and color reproduction in halftone images, modifications of the Murray–Davies

equation are used. In this report, F will refer to the actual, measured dot area fraction rather than the fraction commanded by the printer, and a modification of the Murray–Davies equation that models the Yule–Nielsen effect on color halftones will be described.

The earliest and still most commonly used modification of the Murray–Davies equation is the Yule–Nielsen equation, with an empirical *n* factor.[1]

$$R^{1/n} = F_k R_k^{1/n} + F_p R_p^{1/n}. \tag{1}$$

In this expression, F_k and F_p are the area fractions of the ink dots and the paper between the dots, respectively, and $F_p = 1 - F_k$. The Murray–Davies and Yule–Nielsen equations are often extended to describe spectral reflectance in *cmy* color halftoning.

$$R(\lambda) = \sum_{i=1}^{8} f_i R_i(\lambda), \tag{2}$$

$$R(\lambda)^{1/n} = \sum_{i=1}^{8} f_i R_i(\lambda)^{1/n}. \tag{3}$$

The f_i are the area fractions of the eight possible colors (white, cyan, magenta, yellow, red, green, blue, and black) formed by overlap between the printed ink area fractions c, m, and y. The $R_i(\lambda)$ are the reflection spectra of the eight colors. By knowing or assuming the geometry of overlap between ink dots, the color fraction may be determined from the ink fractions, $f_i = f(c,m,y)$. The most common assumption regarding dot overlap is that dots are printed randomly, which leads to the so-called Demichel equations [$f_1 = (1 - c)(1 - m)(1 - y)$, through $f_8 = c, m, y$].[2] Models for deterministic dot placement have also been published.[3]

By integration, the CIE chromaticity coordinates may be determined.

$$XYZ = \int R(\lambda)\overline{xyz}P(\lambda)d\lambda, \tag{4}$$

where *XYZ* represents the *X*, *Y*, or *Z* chromaticity value and $\overline{xyz}$ represents the corresponding *x*, *y*, or *z* color matching function. The value $P(l)$ is the spectral power distribution of the light used to view the image. By applying Eq. 4 to Eq. 2 we have what is often called the Neugebauer equation for tristimulus values,[2]

$$XYZ = \sum_{i=1}^{8} f_i \cdot XYZ_i^{1/n}, \tag{5}$$

where XYZ_i represents a tristimulus value for the color region *i* of the halftone.

The empirical modification for $R(\lambda)$ may also be

used to calculate tristimulus values. However, Eq. 6 does not follow from application of Eq. 4 to Eq. 3.

$$XYZ^{1/n} = \sum_{i=1}^{8} f_i XYZ_i^{1/n}. \tag{6}$$

Nevertheless, Eq. 6 is occasionally used as an empirical modification of Eq. 5. Because n is only an empirical factor, no reason exists not to use Eq. 6 if it provides a useful description of a given halftone system.[4]

Work in this laboratory has explored an alternative modification to the Murray–Davies equation in which R_i and R_p are not constants but are described as functions of the dot area fraction $R_k(F_k)$ and $R_p(F_p)$.[5]

$$R = F_k R_k(F_k) + F_p R_p(F_p). \tag{7}$$

Experimentally it has been well shown that both R_k and R_p decrease as F_k increases.[5] Both empirical and theoretical models have been reported for describing R_k and R_p versus F_k for monochrome halftones.[5–7]

The Probability Functions

Equation 7 may be expanded to describe *cmy* halftone color. Equation 2 is the appropriate expansion of Eq. 7 if we consider the eight $R_i(\lambda)$ spectra to be functions of the color fractions f_i as well as functions of wavelength λ. Then, integration gives the tristimulus values of the color image. The problem is to describe the way in which the eight $R_i(\lambda)$ of Eq. 2 depend on the eight f_i. The approach taken in this report is to describe probability functions for the lateral scattering of light in the paper and then to describe the way in which the eight R_i spectra depend on the probability functions.

We begin by defining the probability function P_{ji}. This is the probability that if a photon enters the paper in region j, of area fraction f_j, it will reemerge after scattering in region i, of area fraction f_i. In other words, if N photons enter the paper in region i, then P_{ji} is the fraction of these N photons that scatters and emerges in region i, provided no light is absorbed by the paper. To account for light absorption, we assume absorption and scattering probabilities are independent so that the final number of photons from region j that emerges in region i is the product $R_g P_{ji}$.

Consider the monochrome case with region $j = 1$ defined as the region between the dots and region $i = 2$ the region of the paper containing dots. The probability P_{11} is the probability of light emerging from the region between the dots after entering between the dots. For conventional clustered dot halftones this probability was experimentally shown to be well described by the following function[7]:

$$P_{11} = 1 - (1 - f_1)\left[1 - (1 - f_1)^w + (1 - f_1^w)\right], \tag{8}$$

where f_1 is the same thing as F_p in Eq. 7 and w is a factor related to the scattering of light in paper. The w factor has been shown to be related to the scattering optics of the paper,

$$w = 1 - e^{-Ak_p v}, \tag{9}$$

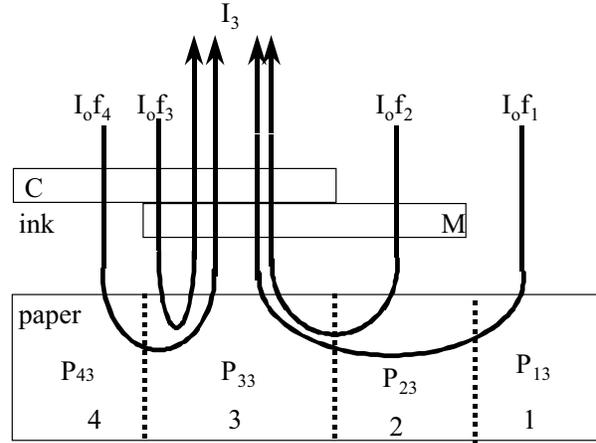where A is a constant characteristic of the halftone ge-

Figure 1. For a two-color (cyan, magenta) halftone, the light reflected back from the blue region has four origins as a result of the Yule–Nielsen effect.

ometry, k_p is a constant proportional to the mean distance light travels in paper before reemerging as reflected light, and n is the halftone dot frequency. A thorough discussion of the terms in Eq. 9 was reported elsewhere.[7]

Equation 8 may be generalized to describe the probability P_{jj} that light that enters an area of the paper marked j will emerge from the paper at area j, with f_j as the area fraction.

$$P_{jj} = 1 - (1 - f_j)\left[1 - (1 - f_j)^w + (1 - f_j^w)\right]. \tag{10}$$

Similarly, an extension of previous work on monochrome FM halftones leads[8] to a somewhat different expression for P_{jj},

$$P_{jj} = 1 - w\left(1 - f_j^B\right), \tag{11}$$

where w is again given by Eq. 9 but with n defined as the inverse of the dot diameter. The B factor is an empirical factor related to the particular geometry of the FM halftone.[8]

In addition to the P_{jj} probabilities, there are also all of the P_{ji} probabilities, as illustrated for the *cy* two-ink case in Fig. 1. If we have functions to describe all of the P_{ji}, then for a three-color *cmy* halftone we would have an 8×8 matrix of probability functions P_{ji} with the P_{jj} functions on the diagonal of the matrix. Similarly, a monochrome halftone would be described with a 2×2 matrix of probability functions. As will be shown below, the P_{ji} can be related to the P_{jj}. First, however, we examine how these probabilities can be used to calculate color reproduction in the halftone.

From Probability to Reflectance

The two-ink case illustrated in Fig. 1, shows how the incident irradiance, I_0 = watts/area, is divided among the areas, f_i, of the halftone image. Photons $I_0 f_i$ strike the image in region number i. The light that then enters the paper in this region is $I_0 f_i T_i$, where T_i is the Beer–Lambert transmittance of the ink layer over region i. Note that $T_i = 0$ for $i = 1$ (the paper between the dots) and that $T_2 = T_{cyan}$, $T_3 = T_{cyan} T_{yellow}$, etc. Then, the number of photons from region i that emerge from region j is $I_0 f_i T_i P_{ji}$. For example, as illustrated in Fig. 1, the number of photons that strike Region 4 (the cyan-color region) and

eventually emerge under Region 3 is given by the product $(I_0 T_4 R_g P_{43})$. The total amount of scattered light that reaches Dot 3 is the sum of these expressions for Regions 1, 2, and 4. Then the light passes through Dot 3 and is attenuated by T_3. Similarly, the general expression for the photon irradiance emerging from any dot i is as follows:

$$I_i = I_0 R_g T_i \sum_J (T_J P_{ji} f_j). \qquad (12)$$

The reflectance of the dot is the ratio of the light emerging from the dot, I_i, to the light entering the dot, $I_0 f_i$. Thus, dividing Eq. 12 by $I_0 f_i$ gives the following expression for the reflectance of dot i.

$$R_i = R_g T_i \sum_J \left(T_J P_{ji} \frac{f_j}{f_i} \right). \qquad (13)$$

The spectral designation (l) has been dropped to simplify the notation, but R_i, R_g, and all the T_j are functions of wavelength. The spectral R_i may then be used in Eq. 2 to determine the overall spectral reflectance of the halftone image, and then Eq. 5 can be used to calculate the tristimulus values of the image. The only unknown in the model is a description of the off-diagonal probabilities P_{ji}.

The Off Diagonal Probabilities

Everything required to model halftone color is now known except the off-diagonal probabilities P_{ji}. Intuitively, the P_{ji} must relate to the P_{jj} and to the color fractions f_j and f_i. We can derive this relationship by assuming the independence of the scattering probabilities P_{ji} and the absorption probabilities T_i and R_g. We also assume the paper is sufficiently thick that loss of light through the back of the paper is negligible. Under these conditions, the photons that enter Region 3 of Fig. 1 must eventually emerge in one of the four regions.

$$P_{13} + P_{23} + P_{33} + P_{43} = 1. \qquad (14)$$

This expression is a special case of Eq. 13 for a two-ink halftone and for $R_g = T_i = T_j = 1$. If we further assume that the dots are randomly placed on the paper so that the probability of light from Region k emerging in some other Region $i \neq k$ is proportional to the area fraction i. Thus, for any two regions $i \neq k$ and $j \neq k$, we may write the following:

$$P_{ki}/P_{kj} = f_i/f_j. \qquad (15)$$

For example $P_{31} = P_{31}(f_1/f_1)$, $P_{32} = P_{31}(f_2/f_1)$, and $P_{34} = P_{31}(f_4/f_1)$. Combining these with Eq. 14 gives the following:

$$P_{31}(f_1/f_1) + P_{31}(f_2/f_1) + P_{31} + P_{31}(f_4/f_1) = 1 \qquad (16)$$

Note that Eq. 15 does not apply to P_{33}, but only to $i \neq j$. Then we recognizing $f_1 + f_2 + f_4 = 1 - f_3$ and solve Eq. 16 for the off-diagonal P_{31}.

$$P_{31} = (1 - P_{33}) \left(\frac{f_i}{1 - f_3} \right). \qquad (17)$$

We may generalize this expression for any off-diagonal term, $i \neq j$.

$$P_{ji} = (1 - P_{jj}) \left(\frac{f_i}{1 - fj} \right). \qquad (18)$$

We now have a sufficient set of functions to model color halftones.

The Model Recipe

To apply these probability functions to calculate the XYZ tristimulus values of a color halftone given the c, m, and y ink fractions delivered by a printer, the following steps are taken: (Note c, m, and y are the actual areas not the areas commanded by the printer. Physical dot gain is not considered here.)

Step 1. Measure the transmittance spectra of the individual inks, T_{cyan}, $T_{magenta}$, and T_{yellow}. Assume the Beer–Lambert law and determine the transmittance spectra T_i of the eight colors. Also measure the reflection spectrum of the paper, R_g.

Step 2. Begin with the ink combination (c, m, y) and calculate the eight color fractions, f_1 through f_8. For randomly placed ink dots, the Demichel equations may be used. Otherwise dot geometry must be modeled, as illustrated for dot-on-dot halftones described subsequently.

Step 3. Use Eq. 10 to calculate the eight diagonal probabilities, P_{jj}, for a traditional clustered dot halftone. Eq. 11 may be used with an FM, stochastic type of halftone. The parameters w and B may be taken as arbitrary constants to fit the model to data. Alternatively, w and B may be measured independently as described previously.[8]

Step 4. Use Eq. 18 to calculate the off-diagonal probabilities.

Step 5. Use Eq. 13 to calculate the reflection spectra of the eight colors.

Step 6. Use Eq. 2 to calculate the reflection spectrum of the overall halftone image.

Step 7. Use Eq. 5 and the power spectrum of the illumination light, $P(l)$, to calculate the XYZ tristimulus values of the halftone image.

Testing the Model

Color halftones were generated with an HP 1600C ink-jet printer on a high-quality coated sheet to minimize ink penetration and dot gain. Halftones were printed with an error diffusion algorithm, and dot-on-dot was not used. The dots from the different colors were at 300 dpi and were randomly placed with respect to each other. A fixed amount of magenta (dot fraction m = 0.45) was printed at different cyan dot fractions ($0 < c < 1$). No yellow was printed in this experiment. A microscopic image of the dot pattern was captured with a 2-mm field of view using a 3-chip color CCD camera and video frame grabber. The sample was illuminated with an incandescent light source through fiber optics. The resulting light on the sample was measured and found to have the power distribution $P(\lambda)$ of CIE Illuminant A. The camera and optical system had been calibrated to the ink-jet dye set so the rgb images could be translated into XYZ space. In
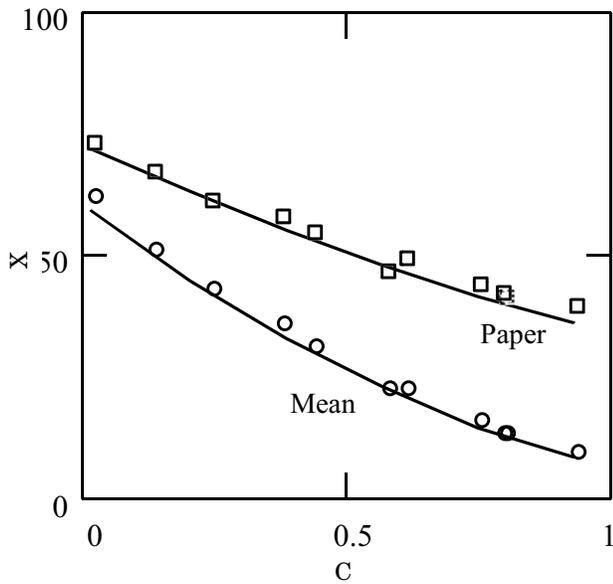
Figure 2. The X tristimulus value of the paper between the dots (□) and of the overall, mean value of the halftone image (O) versus the ink area fraction of cyan at magenta = 0.45. Error diffusion halftone at 300 dpi.
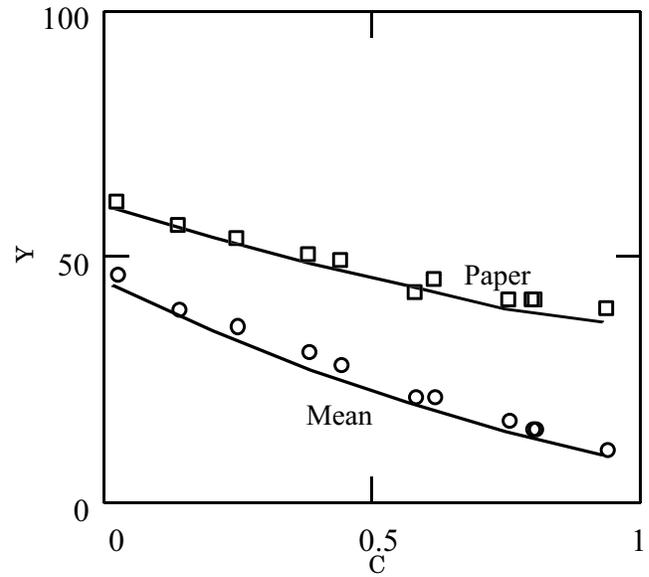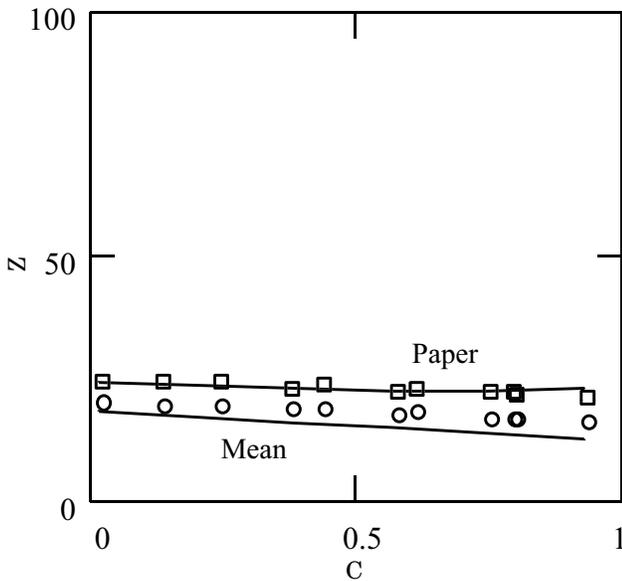

Figure 3. The Y tristimulus value of the paper between the dots (□) and of the overall, mean value of the halftone image (O) versus the ink area fraction of cyan at magenta = 0.45. Error diffusion halftone at 300 dpi.

Figure 4. The Z tristimulus value of the paper between the dots (□) and of the overall, mean value of the halftone image (O) versus the ink area fraction of cyan at magenta = 0.45. Error diffusion halftone at 300 dpi.
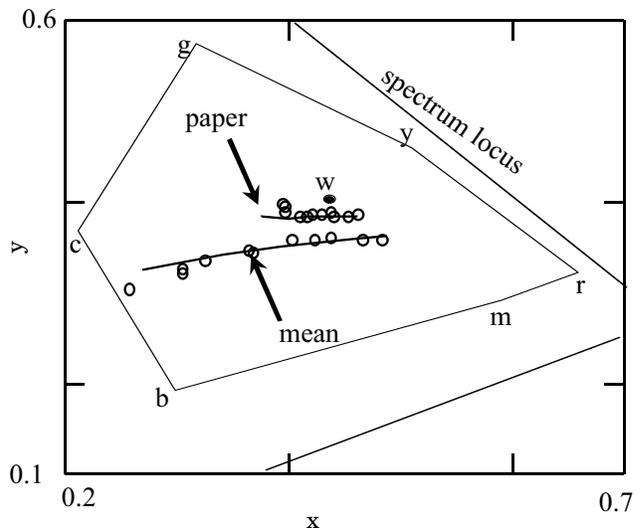

Figure 5. The xy chromaticity trajectory with Illuminant A for the paper between the dots and for the overall image for the variable cyan, fixed magenta, error diffusion halftone. The gamut of the printer at maximum c, m, and y inks is shown. The paper chromaticity (w ●) and the spectrum locus are shown.

addition, gray-level segmentation in the original rgb images provided independent measures of the c, m, and y dot area fractions. Using the color microdensitometer, measurements were made of the *XYZ* tristimulus values of not only the overall image but of the space between the ink dots. The results were plotted as a function of the cyan dot area fraction c and are shown in Figs. 2, 3, and 4. Figure 5 shows the corresponding x,y chromaticity values. The data do not go all the way to the gamut limit because the printer, at a command of 100% ink, formed dots with very little dot gain and occupied only

90% of the paper area. The model was run over the range $0 < c < 0.9$ to agree with the experiment. These experiments demonstrate that the color between the dots is, indeed, not the color of the unprinted paper but mimics the mean value color of the overall image.

The solid lines in Figs. 2 through 5 were calculated with the model recipe described above. The transmittance spectrum of the cyan dye was determined from the reflection spectrum, R_{cyan}, of a 100% cyan region ($m = y = 0$) and the function, $T_{cyan} = (R_{cyan}/R_g)^{1/2}$. Spectra for the magenta and yellow were similarly determined. The Demichel
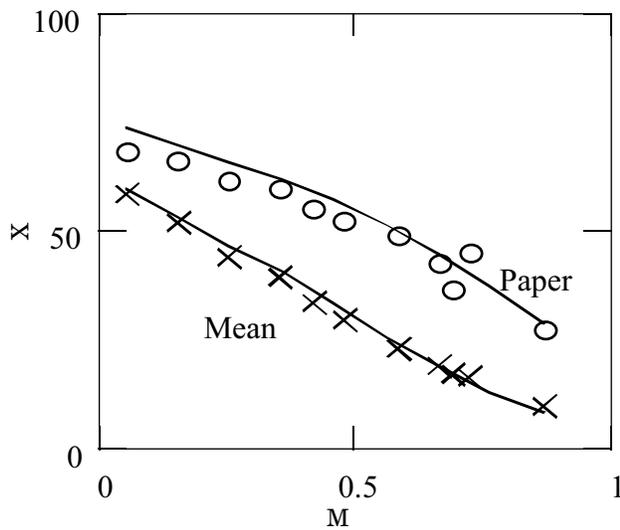
Figure 6. The X tristimulus value of the paper between the dots (O) and of the overall, mean value of the halftone image (X) versus the ink area fraction of cyan at magenta = 0.4. Clustered dot-on-dot halftone at 53 dpi.
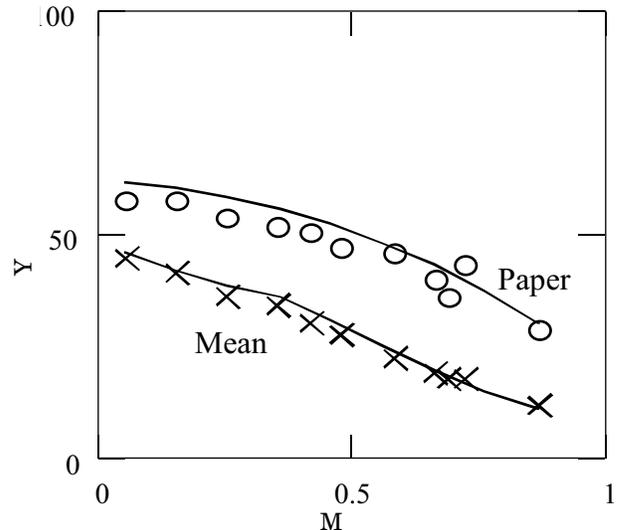

Figure 7. The Y tristimulus value of the paper between the dots (O) and of the overall, mean value of the halftone image (X) versus the ink area fraction of cyan at magenta = 0.4. Clustered dot-on-dot halftone at 53 dpi.
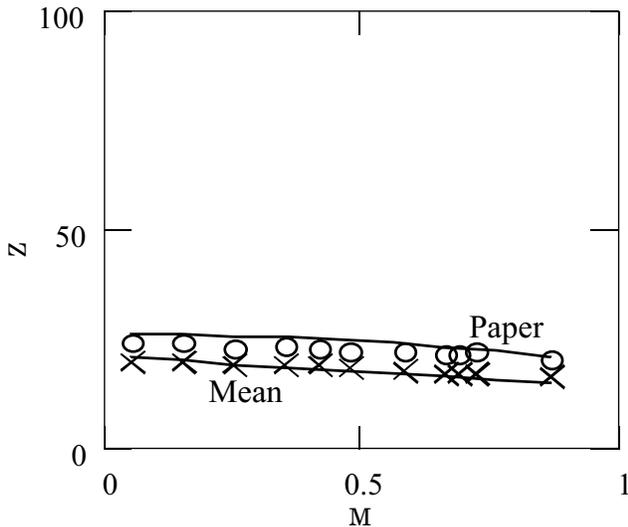

Figure 8. The Z tristimulus value of the paper between the dots (O) and of the overall, mean value of the halftone image (X) versus the ink area fraction of cyan at magenta = 0.4. Clustered dot-on-dot halftone at 53 dpi.
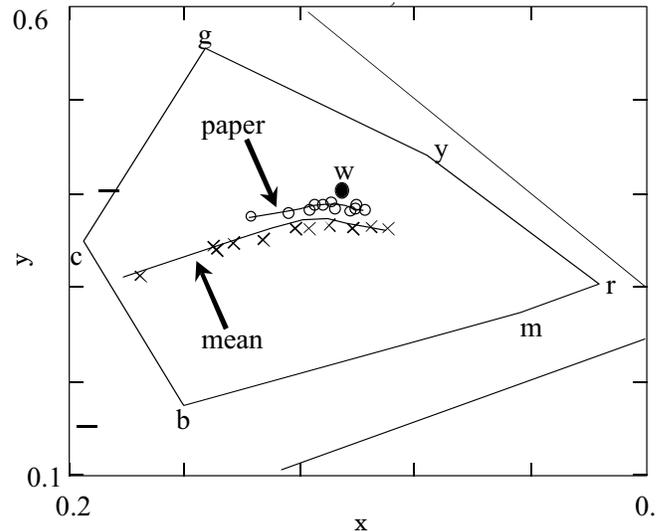

Figure 9. The xy chromaticity trajectory with Illuminant A for the paper between the dots and for the overall image for the variable cyan, fixed magenta, clustered dot-on-dot halftone. The gamut of the printer at maximum c, m, and y inks is shown. The paper chromaticity (w ●) and the spectrum locus are shown.

equations were used to determine the color area fractions f_i, and Eq. 11 for FM halftones was used for the on-diagonal probabilities. The model was fit to the data by adjusting w and B. Rather than search for a statistical fit criteria, the authors simply adjusted w and B to achieve a visually acceptable agreement between the model and all of the data in Figs. 2 through 5. Values of $w = 0.82$ and $B = 1.2$ were used in this calculation and are consistent with independent estimates from earlier work.[8,9]

A second experiment was performed using the same inks and a traditional clustered dot halftone. However, the clustered dot halftone was printed dot-on-dot rather than randomly. Figures 6 through 9 show the results. Again the color of the paper between the dots mimics the color of the halftone image. The solid lines in these figures were modeled by the recipe above with the following changes. First, Eq. 10 was used for the diagonal probabilities. Second, the Demichel equations were replaced with a geometric calculation for dot-on-dot halftones. For the fixed magenta at different levels of cyan, the functions in Table I were used. The value of $w = 0.80$ was found to provide an overall fit, judged visually, to the data in Figs. 6 through 9.

Discussion

As shown by Engeldrum, the Yule–Nielsen effect manifests itself in color halftones as a change in the color of the paper between the halftone dots as the dot area fractions change.[10,11] The probability model appears to pro-

vide a mechanistic rational for this phenomenon. More-over, the model rationalizes the overall color of the half-tone image. The printer used in the project employed a default algorithm for gray color removal, and this prevented experimental testing with more than two of the three *cmy* inks. However, the fit with the two color cases strongly supports the model. This, in turn, indicates that the Neugebauer Eqs. 2 and 5 are correct descriptions of halftone color reproduction provided the eight reflectance spectra R_i and the eight sets of tristimulus values XYZ_i are treated as continuous functions of ink fractions *cmy* and not as the reflectance spectra and tristimulus values of the eight Neugebauer colors printed at 100% coverage. This point is emphasized by integrating Eq. 13 directly to find the eight sets of Neugebauer tristimulus values to use in Eq. 5. Integration leads to the following:

$$XYZ = \sum_{j=1}^{8} \left[P_{ij} XYZ_{ij} \frac{f_j}{f_i} \right]. \qquad (19)$$

Note that integration leads to a matrix of 64 tristimulus values XYZ_{ij}. The eight values on the diagonal XYZ_{jj} are the traditional Neugebauer values for the eight Neugebauer colors printed at 100% coverage.[2,11] These values may be measured independently. However, the off-diagonal values XYZ_{ij} are tristimulus values for light that passes Dot *j*, scatters in the paper, and then passes through Dot *i*. The XYZ_{ij} tristimulus values can not be measured independently.

Unlike the Yule–Nielsen modification to the Neugebauer equation, the probability model has a direct link with the fundamental optical and geometric characteristics of the halftone system via Eq. 9. While the probability model is significantly more complex than the traditional *n* modified Yule–Nielsen model, it is significantly less complex than a convolution model involving the fundamental probability function PSF of light in the paper. Gustavson[12] has demonstrated such a model, and it is fundamentally correct theoretically. However, the current probability model is expressed with closed analytical functions and is much more amenable to modifications for nonideal systems, as demonstrated in previous work.[9] Moreover, one should be able to derive the mean level probabilities P_{jj} from the fundamental probability *PSF* and a knowledge of the geometry of the halftone system. Because the PSF of paper is quite difficult to measure experimentally, it is typically modeled empirically. In the current model, we begin by modeling P_{jj} empirically. In addition, as demonstrated previously,[8] it may be easier to measure the P_{jj} than the PSF. Thus, one experimental approach to measuring PSF may be to measure P_{jj} with several known dot geometries and then to calculate PSF.

Appendix

A reviewer of this manuscript correctly pointed out that Eq. 15 implies an assumption. The assumption is that the off-diagonal probabilities P_{ik} are proportional to the area fractions f_i so that $P_{ik} = a_k f_i$, for $i \neq k$. If a nonlinear proportionality actually applies so that $P_{ik} = a_k G(f_i)$ for some function G, then Eqs. 15 through 18 become more complex. While this may certainly be the case, it is not revealed in the experimental data and the data are not sufficiently noise-free to provide a guide to a more advanced estimate of the functional form of Eq. 15. For a more rigorous analysis of this probability, the reader is directed to recent theoretical work by Rogers.[13–15]

Acknowledgments

References

1. J. A. Yule and W. J. Nielsen, *TAGA Proc*. p. 65 (1951).
2. J. A. Yule, *Principles of Color Reproduction*, Chap. 10, John Wiley & Sons, NY, 1967, p. 255.
3. T. N. Pappas, *Proc. IS&T* **47,** 468 (1994).
4. J. A. S. Viggiano, *TAGA Proc*. **37,** 647 (1985).
5. J. S. Arney, P. G. Engeldrum and H. Zeng, An expanded Murray–Davies model of tone reproduction in halftone imaging, *J. Imaging Sci. Technol*. **39,** 502 (1995); *see pg. 390, this publication*.
6. J. S. Arney, C.D. Arney and P. Engeldrum, Modeling the Yule–Nielsen halftone effect, *J. Imaging Sci. Technol*. **40,** 233 (1996); *see pg. 432, this publication*.
7. J. S. Arney, A probability description of the Yule–Nielsen effect, *J. Imaging Sci. Technol*. **41,** 633 (1997); *see pg. 451, this publication*.
8. J. S. Arney and M. Katsube, A probability description of the Yule–Nielsen effect II: The impact of halftone geometry, *J. Imaging Sci. Technol*. **41,** 637 (1998); *see pg. 456, this publication*.
9. M. Alber, *Modeling the effect of ink spread and penetration on tone reproduction*, M.S. Dissertation, Rochester Inst. of Technol., Rochester, NY, 1997.
10. P. G. Engeldrum and B. Pridham, Application of turbid medium theory to paper spread function measurements, *TAGA Proc*. **47,** 353 (1995).
11. P. G. Engeldrum, The color gamut limits of halftone printing with and without the paper spread function, *J. Imaging Sci. Technol*. **40,** 240 (1996); *see pg. 426, this publication*.
12. S. Gustavson, Color gamut of halftone reproduction *J. Imaging Sci. Technol*. **41,** 283 (1997); *see pg. 443, this publication*.
13. G. L. Rogers, Optical Dot gain in a halftone print, *J. Imaging Sci. Technol*. **41,** 643 (1997); *see pg. 462, this publication*.
14. G. L. Rogers, Optical dot gain: Lateral scattering probabilities, *J. Imaging Sci. Technol*. **42**(4)**,** 341-345 (1998); *see pg. 495, this publication*.
15. G. L. Rogers, The effect of light scatter on halftone color, *J. Opt. Soc. Am. A*. **15,** 1813 (1998).

❋ Previously published in the *Journal of Imaging Science and Technology* **42**(4), pp. 335–340, 1998.